

Design and performance of a gain calibration system for the POLARBEAR-2a receiver system at the Simons Array cosmic microwave background experiment

Daisuke Kaneko^{a,*†}, Sayuri Takatori^{b,c,*†}, Masaya Hasegawa^{a,c},
Masashi Hazumi^{a,c,d,e}, Yuki Inoue^f, Oliver Jeong^g, Nobuhiko Katayama^e,
Adrian T. Lee^{g,h}, Frederick Matsuda^d, Haruki Nishinoⁱ, Praween Siritanasak^{b,j},
Aritoki Suzuki^{b,h}, Satoru Takakura^{b,k}, and Takayuki Tomaru^l

^aHigh Energy Accelerator Research Organization, International Center for
Quantum-field Measurement Systems for Studies of the Universe and Particles, Tsukuba, Japan

^bOkayama University, Research Institute for Interdisciplinary Science, Okayama, Japan

^cHigh Energy Accelerator Research Organization, Institute of Particle and Nuclear Studies, Tsukuba, Japan

^dJapan Aerospace Exploration Agency, Institute of Space and Astronautical Science, Sagami-hara, Japan

^eUniversity of Tokyo, Kavli Institute for the Physics and Mathematics of the Universe, Kashiwa, Japan

^fNational Central University, Center for High Energy and High Field Physics, Department of Physics, Taoyuan,
Taiwan

^gUniversity of California, Department of Physics, Berkeley, California, United States

^hLawrence Berkeley National Laboratory, Physics Division, Berkeley, California, United States

ⁱThe University of Tokyo, Graduate School of Science, Research Center for the Early Universe, Tokyo, Japan

^jNational Astronomical Research Institute of Thailand, Chiangmai, Thailand

^kKyoto University, Department of Physics, Faculty of Science, Kyoto, Japan

^lNational Astronomical Observatory of Japan, Gravitational Wave Project Office, Mitaka, Japan

ABSTRACT. We present an advanced system for calibrating the detector gain responsivity with a chopped thermal source for POLARBEAR-2a, which is the first receiver system of a cosmic microwave background (CMB) polarimetry experiment: the Simons Array. Intensity-to-polarization leakage due to calibration errors between detectors can be a significant source of systematic error for a polarization-sensitive experiment. To suppress this systematic uncertainty, POLARBEAR-2a calibrates the detector gain responsivities by observing a chopped thermal source before and after each period of science observations. The system includes a high-temperature ceramic heater that emits blackbody radiation covering a wide frequency range and an optical chopper to modulate the radiation signal. We discuss the experimental requirements of gain calibration and system design to calibrate POLARBEAR-2a. We evaluate the performance of our system during the early commissioning of the receiver system. This calibration system is promising for the future generation of CMB ground-based polarization observations.

© The Authors. Published by SPIE under a Creative Commons Attribution 4.0 International License. Distribution or reproduction of this work in whole or in part requires full attribution of the original publication, including its DOI. [DOI: [10.1117/1.JATIS.10.1.018003](https://doi.org/10.1117/1.JATIS.10.1.018003)]

Keywords: cosmic microwave background; gain calibrator; detector calibration; transition edge sensor

Paper 23090G received Aug. 7, 2023; revised Nov. 2, 2023; accepted Dec. 14, 2023; published Jan. 27, 2024.

*Address all correspondence to Daisuke Kaneko, dkaneko@post.kek.jp; Sayuri Takatori, takatori@okayama-u.ac.jp

†These authors contributed equally to this work.

1 Introduction

The precise measurement of cosmic microwave background (CMB) polarization, particularly the spatially odd-parity polarization pattern called “*B*-mode,” is crucial for exploring the early universe. The *B*-modes at the degree scale reveal the primordial gravitational waves from inflation in the early universe,^{1,2} and their precise measurement leads to quantitative studies such as the energy scale when it occurs. In addition, the *B*-modes at the subdegree scale are sensitive to the weak gravitational lensing effect. Precise measurements of the lensing *B*-modes provide unique information on the large-scale structure of the universe, which also allows us to constrain the sum of the neutrino masses.^{3,4}

Mitigating the systematic errors in the observations is crucial for achieving precise measurements of CMB polarization. One of the major systematic errors is due to the uncertainty of the detector gains (responsivities). In CMB polarization observations, pairs of two orthogonal detectors are commonly used. If the gains of the two detectors are incorrectly calibrated, fake polarization signals are generated. This systematic error can be mitigated by improving the precision of the gain calibration.

Various gain calibration methods have been developed for CMB polarization observations.^{5–10} Calibration periods are important because gain fluctuations occur at every time scale owing to a fluctuation of the observation apparatus and atmosphere. The actual gain calibration strategy is determined by considering the performance and utility of the methods. The detector gain is finally calibrated by the temperature of the blackbody spectrum that best fits the CMB power spectrum. However, this requires observing a specific sky area for a sufficient duration. Hence, additional methods are required to track daily gain changes. Observations of celestial objects, such as planets, can provide constant sources but are not always performed owing to the daily changes in their positions and the sky conditions. Injecting a stable optical signal from a thermal source into the detectors is useful for calibrating the relative gain change in the time range from hours to days.

This study aims to mitigate the uncertainty of detector gains for the Simons Array (SA) experiments^{11–13} through the use of a reference thermal source. The SA is a ground-based CMB polarization experiment in the Atacama Desert, Chile, at an altitude of 5200 m. It is an upgraded version of the POLARBEAR (PB-1) experiment.^{5,14,15} The projected constraint at the SA on the tensor-to-scalar ratio r is expected to be $\sigma(r) = 0.006$ at $r = 0.1$, and the sensitivity to the sum of the neutrino masses is expected to be 40 meV (68% C.L.).^{13,16} POLARBEAR-2a (PB-2a) is the first of three-receiver systems in the SA.^{13,16,17} The PB-2a focal plane contains 7588 transition edge sensor (TES) bolometers¹⁸ connected to a broadband antenna and simultaneously observes the 90 and 150 GHz bands for foreground subtraction.

We have developed a gain calibrator, a “stimulator,” for PB-2a. The stimulator is designed to simultaneously calibrate the gains of all TES bolometers in two observation frequency bands, using blackbody radiation from the thermal source covering a wide range of observation frequencies. The same type of calibrator was used in some CMB polarization experiments,^{5,19,20} and the design of the PB-2a stimulator is based on PB-1 equipment (Appendix A) in many respects. In this study, we detail its construction, operation, and validation of the stimulator.

The remainder of this paper is organized as follows. We introduce the general TES gain calibration in the CMB polarization observation in Sec. 2 and discuss the gain calibration requirements for PB-2a in Sec. 3 and Appendix B. Sections 4 and 5 explain the design and operation of the stimulator. Sections 6 and 7 summarize the performance evaluation during the early commissioning. In Appendix C, we discuss a case where the stimulator is used with a polarization modulator for future applications.

2 Formulation of Gain Calibration

The gain of a detector is defined as a factor that connects the detector’s electrical output to the sky optical power. In CMB experiments, TES types of bolometers are widely used. TES bolometers read the incident optical power as a current value as

$$I(\omega) = R_{\text{det}}(\omega)P_{\text{opt}}(\omega), \quad (1)$$

where ω is the angular frequency of signal fluctuation and a bolometer’s responsivity R_{det} is

$$R_{\text{det}}(\omega) = -\frac{\sqrt{2}\eta}{V_{\text{bias}}} \frac{\mathcal{L}}{\mathcal{L} + 1} \frac{1}{1 + i\omega\tau}, \quad (2)$$

where η is the optical efficiency, V_{bias} is the RMS of AC bias voltage, \mathcal{L} is the loop gain, and τ is the time constant of the TES bolometer.^{21,22} Here the optical efficiency depends on the telescope optics and the detector bandpass. The bias voltage is affected by the temperature of the focal plane and the optical loading from the atmosphere. The loop gain depends on the operation resistance of the TES bolometer. The time constant, depends on the loop gain, and its value for each bolometer should be determined through measurement. The calibration of R_{det} is typically challenging and imprecise. Instead, we opt to calibrate the overall gain using optical reference signals.

2.1 Introduction of PB-2a Stimulator

The PB-2a stimulator was designed to be placed on the telescope as illustrated in Fig. 1. The stimulator is equipped with a ceramic heater inside. Wide frequency bandwidth optical signals are available by modulating a blackbody radiation source of ~ 1000 K with a chopper of ~ 300 K at arbitrary modulation speeds. The role of the stimulator is to evaluate the factor, which converts the input optical power to the temperature (in Kelvin unit) of the sky and to measure the time constant of the TES bolometers.

The gain measured with the stimulator is calculated as $G := R_{\text{det}}(P_{\text{stm}}/T_{\text{stm}}) = I_{\text{stm}}/T_{\text{stm}}$, where I_{stm} is the signal amplitude of the output current with the stimulator, and T_{stm} is the effective temperature of the stimulator. T_{stm} is defined with a situation in which a blackbody of a certain temperature fills the entire field-of-view of the TES bolometers. The signal from the stimulator is assumed to be equal to that from the blackbody. During CMB observation periods, gain calibrations are performed before and after each observation scan (typically over several hours) to evaluate the gain variation. The gain is assumed to change slowly and linearly during the observation scan, and the change could be calibrated by interpolation of calibrations.

The effective temperature T_{stm} is corrected every few days using planets,²³ as the temperatures of those stellar objects are expected to be more stable. It is obtained by comparing the outputs from the stimulator and the planet. The detailed method is explained in Sec. 6.1.

To accomplish the gain calibration by converting T_{stm} to the sky optical temperature, we use the best fit of the WMAP-9 and the Planck power spectrum of CMB temperature anisotropies $C_{\ell,\text{ref}}^{\text{TT}}$ ^{24,25} such that the observed anisotropies $C_{\ell,\text{obs}}^{\text{TT}}$ match with reference $C_{\ell,\text{ref}}^{\text{TT}}$, and this paper is not primarily focused on the detailed method used to obtain the absolute gain for the subsequent physical analysis.

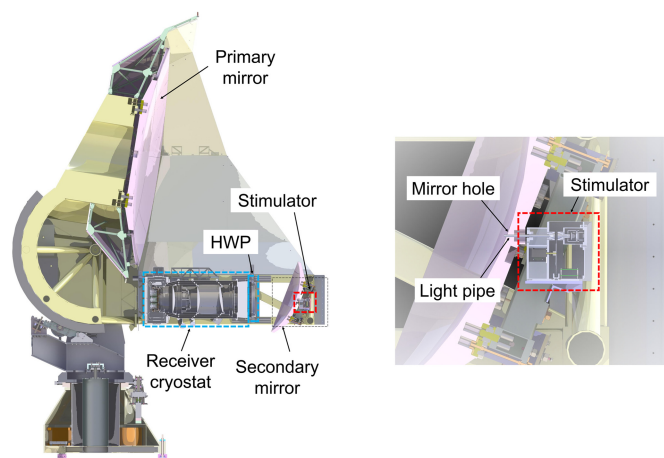


Fig. 1 Cross-sectional image of the stimulator on the PB-2a telescope. The figure on the right side provides a zoomed-in view around the stimulator. The stimulator was placed behind the secondary mirror. Its light covers the detectors on the focal plane through a light pipe penetrating a 9-mm diameter hole in the secondary mirror.

2.2 Gain Measurement with Stimulator

The electrical output for the stimulator signal is written as $I_{\text{obs}} = G \cdot T_{\text{stm}} + I_{\text{noise}}$. Here I_{noise} represents the noise on the bolometer. The error in the gain estimation originates from an uncertainty of the stimulator signal and the bolometer noise in the electrical output. The uncertainty of the stimulator signal is proportional to the fluctuation of the stimulator heater temperature δT_{stm} . The noise of the electrical output can be written as $\delta I_{\text{obs}} = G \cdot \text{NET}_{\text{bolo}} / \sqrt{t_{\text{obs}}}$, where NET_{bolo} represents the noise equivalent temperature of the bolometer, and t_{obs} is the time spent on calibration. Therefore, the gain error is expressed as follows:

$$\delta g := \frac{\delta G}{G} = \sqrt{\left(\frac{\delta T_{\text{stm}}}{T_{\text{stm}}}\right)^2 + \left(\frac{\delta I_{\text{obs}}}{I_{\text{obs}}}\right)^2} = \sqrt{\left(\frac{\delta T_{\text{stm}}}{T_{\text{stm}}}\right)^2 + \left(\frac{\text{NET}_{\text{bolo}}}{T_{\text{stm}} \sqrt{t_{\text{obs}}}}\right)^2}. \quad (3)$$

Here $\delta T_{\text{stm}}/T_{\text{stm}}$ denotes the stimulator signal fluctuation. When $\delta T_{\text{stm}}/T_{\text{stm}}$ can be regarded sufficiently small, the following equation holds:

$$\delta g_{\text{bolo}} \sim \frac{\text{NET}_{\text{bolo}}}{T_{\text{stm}} \sqrt{t_{\text{obs}}}}. \quad (4)$$

Let δg_{array} be the relative array error averaged over all detectors. Under the assumption of independent error in each channel, $\delta g_{\text{array}} = \delta g_{\text{bolo}} / \sqrt{N_{\text{bolo}}}$ stands, where N_{bolo} is the number of bolometers. When the array noise $\text{NET}_{\text{array}} \approx \text{NET}_{\text{bolo}} / \sqrt{N_{\text{bolo}}}$ is sufficiently small, δg_{array} can be written as follows:

$$\delta g_{\text{array}} \sim \frac{\delta T_{\text{stm}}}{T_{\text{stm}}}. \quad (5)$$

2.3 Time Constant Measurement with Stimulator

Another role of the stimulator is to evaluate the time constant due to the delay of the TES including electrothermal feedback. The time constant is measured as the decrease in amplitude observed at higher modulation frequencies. The observed signal with time constant τ (s) agrees well with the one-pole response function. It is written as follows:

$$I_{\text{obs}}(\tau) = \frac{G \cdot T_{\text{stm}}}{\sqrt{1 + (2\pi\tau f)^2}}, \quad (6)$$

where f (Hz) denotes the signal-modulation frequency of the stimulator.

3 Calibration Requirements for POLARBEAR-2a

In this section, we estimate the required value of the instrument for measuring the gain variation at each observation.

First, we explain the effect of the gain uncertainty on the CMB polarization observation. Let I be the electrical output from the bolometer. The output of the j 'th bolometer is described using the gain G_j as follows:

$$I_j = G_j [T + (Q \cos 2\phi_j + U \sin 2\phi_j)], \quad (7)$$

where T , Q , and U are the Stokes parameters of the optical source to be observed; T represents the nonpolarized component, which is also called intensity or temperature; Q and U represent linearly polarized components; and ϕ_j is the polarization angle of the antenna.

The sky parameters T , Q , and U are reconstructed from the measured I_j . In this regard, the detector gain G_j must be known. However, in general, the measured gain G_j' has an error. Let us define a fractional gain error δg_j as $\delta g_j := (G_j' - G_j) / G_j'$. The differentiation of the pair of orthogonal detectors provides linear polarization signals. In the case of two orthogonal detectors [their gains are $G_j (j = 1, 2)$], the difference between the two calibrated outputs is described as follows:

Table 1 Summary of the requirements for the stimulator. Required value and fluctuation on the value are illustrated for each requirement. Here the T_{stm} is assumed to be corrected with heater thermometer. The temperature unit is assumed to be calibrated with the temperature of the black-body spectrum of the CMB.

Item	Magnitude	Fluctuation	Section No.
(A) Intensity-to-polarization leakage	$T_{\text{stm}} > 0.1 \text{ mK}$	$\delta T_{\text{stm}}/T_{\text{stm}} < 0.66\% \text{ (1 obs)}$	10.1
(B) Monitoring gain variation	$T_{\text{stm}} > 3 \text{ mK}$	$\delta T_{\text{stm}}/T_{\text{stm}} < 1\% \text{ (1 obs)}$	10.2
(C) Designed time constant value	$T_{\text{stm}} > 5 \text{ mK}$	–	10.3
(D) Relative gain error < absolute gain error	$T_{\text{stm}} > 0.1 \text{ mK}$	$\delta T_{\text{stm}}/T_{\text{stm}} < 0.76\% \text{ (1 obs)}$ $\delta T_{\text{stm}}/T_{\text{stm}} < 0.03\% \text{ (1 season)}$	10.4 –
(E) Modulation frequency for τ measurement	$f_{\text{max}} \gtrsim 44 \text{ Hz}$	$\delta f/f < 1\%$	10.5
(F) Encoder timing readout	–	$\delta t_{\text{chop}} < 0.1 \text{ ms}$	10.6

$$\begin{aligned}
\frac{1}{2} \left(\frac{I_1}{G'_1} - \frac{I_2}{G'_2} \right) &= \frac{1}{2} \left(\frac{G_1}{G'_1} - \frac{G_2}{G'_2} \right) T + \frac{1}{2} \left(\frac{G_1}{G'_1} \cos 2\phi_1 - \frac{G_2}{G'_2} \cos 2\phi_2 \right) Q \\
&\quad + \frac{1}{2} \left(\frac{G_1}{G'_1} \sin 2\phi_1 - \frac{G_2}{G'_2} \sin 2\phi_2 \right) U \\
&= - \left(\frac{\delta g_1 - \delta g_2}{2} \right) T + \cos 2\phi_1 \left(1 - \frac{\delta g_1 + \delta g_2}{2} \right) Q + \sin 2\phi_1 \left(1 - \frac{\delta g_1 + \delta g_2}{2} \right) U, \quad (8)
\end{aligned}$$

where $\phi_1 - \phi_2 = \pi/2$. Ideally, the gains are properly calibrated: $\delta g_1 = \delta g_2 = 0$ holds. In such a case, the first term in the last line of Eq. (8) vanishes, and thus no systematic errors are present. However, when $\delta g_1 \neq \delta g_2$, a polarized component is induced from T even without Q and U . This is referred to as intensity-to-polarization leakage.

To mitigate the uncertainty of gains in each observation by measuring, we list the signal requirements including intensity and stability of the stimulator, as items (A) to (F) in Table 1. All these items must be satisfied to accomplish the calibration. For detailed estimates regarding each item, refer to Appendix B (Secs. 10.1–10.6). In this case when a continuously rotating half-wave plate (HWP) is used, the list of the requirements is modified. It is discussed in Appendix C. Subsequently, we assume the following parameters unless otherwise specifically remarked. The noise level of a single bolometer: $\text{NET}_{\text{bolo}} = 360 \mu\text{K}\sqrt{\text{s}}$,^{11,17} measurement time: $t_{\text{obs}} = 120 \text{ s}$, maximum chopper frequency: $f_{\text{max}} = 44 \text{ Hz}$ (refer to Sec. 5), and time constant of TES: $\tau = 1 \text{ ms}$ as the expected range is 1 to 5 ms.²⁶

The requirement values for the stimulator are summarized in Table 1. In particular, the intensity of the stimulator must be $> 5 \text{ mK}$ [from item (C)]. The stimulator's signal fluctuation must be smaller than 0.66% [from item (A)] in one observation scan and 0.03% [from item (D)] in one observation season (a year). The requirement on the season stability assumes that the heater temperature will be corrected using monitoring with thermometers.

4 Instrument Design

4.1 Thermal Source

Figure 2 shows the schematic of the PB-2a stimulator. We selected a ceramic (alumina) heater (Sakaguchi MS-1000; maximum operation temperature, 1000°C, maximum voltage, 100 V AC, $25 \times 25 \text{ mm}^2$ area) as a radiator because it can tolerate sufficiently high temperatures and is sufficiently large to cover the hole on the secondary mirror (diameter, 9 mm). The effective stimulator temperature T_{stm} was approximated as $(1/2)(T_{\text{heater}} - T_{\text{chop}})(A_{\text{pipe}}/A_{\text{beam}})$, where T_{heater} and T_{chop} are a temperature of the heater surface and the chopper wheel, respectively. A_{pipe} and A_{beam} correspond to the area of the light pipe and the beam spot size on the secondary mirror, respectively.

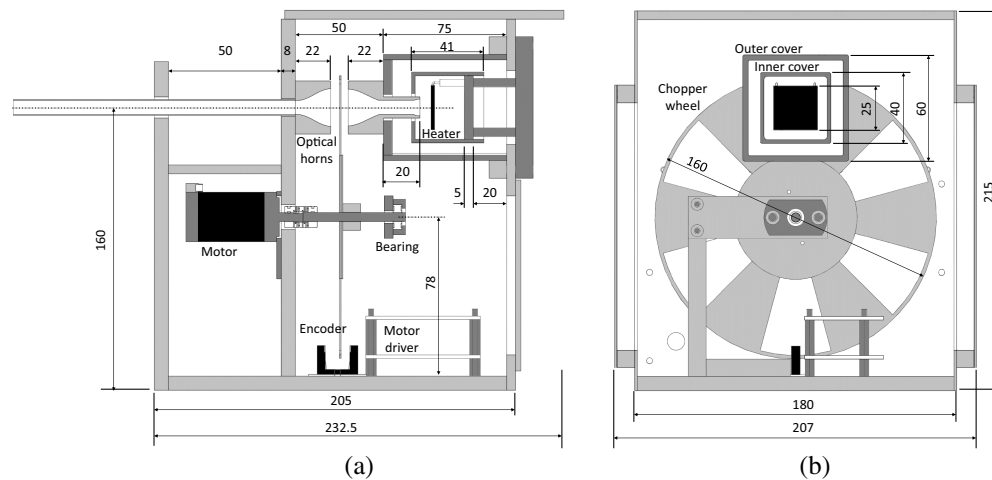


Fig. 2 Cross-sectional image of the PB-2a stimulator. Images in two different planes are shown. Units are in millimeters. (a) A plane parallel to the optical axis. (b) A plane perpendicular to the optical axis and including the heater.

Substituting them with the designed values, the temperature T_{stm} was approximated as $46 \text{ mK}_{\text{RJ}}$. Here K_{RJ} is thermodynamical Rayleigh–Jeans Kelvin temperature.

The heater was enclosed with inner and outer covers to improve thermal stability and prevent the heating of other components. The nominal operating voltage of the heater was set to 40 V. The power consumption of the heater was $\sim 31 \text{ W}$, and the temperature was $\sim 960 \text{ K}$ at the nominal voltage. At the maximum tolerable voltage, the radiation intensity from the heater was high; however, the lifetime of the source heater was short. The nominal voltage was adjusted to consider this trade-off.

4.2 Optical Design

The basic idea of the optical system is to maximize the optical efficiency of the heater within the limited space behind the secondary mirror. Several types of optical systems have been considered. Crucial aspects of these are that (a) the chopper wheel is positioned perpendicular to the optical axis, or with a slanted angle, and (b) absorbers are applied on the surface of the detector side of the chopper.

Consequently, we selected a perpendicular chopper without an absorber. In this configuration, the mechanism is the simplest; thus, the size and cost can be minimized. Conversely, the back-traced rays from the detector are reflected at the chopper and return to the receiver side; hence, the effective temperature is uncertain because predicting where these rays terminate is challenging. Therefore, the stability of the reflection must be verified.

The selected design is illustrated in Fig. 3. A reflective straight pipe with a minimum wall thickness (inner diameter, 8 mm) was used as the light pipe, and an optical horn (Winston cone

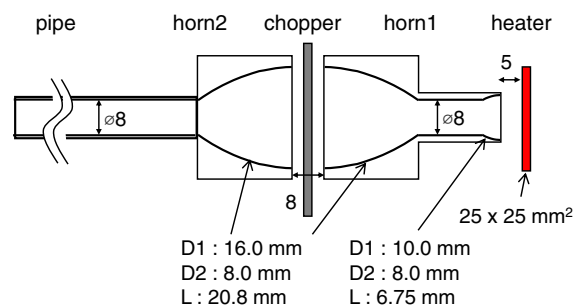


Fig. 3 Internal optical system of the stimulator. We applied the optical horns (Winston cone horn) at the heater and both sides of the gap for improving optical efficiency. Note that the figure is not to scale.

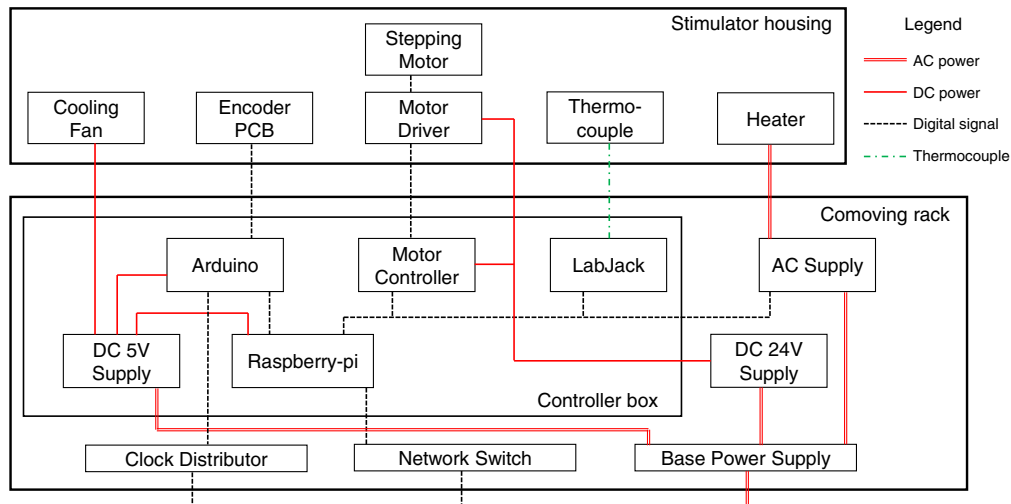


Fig. 4 Connection diagram of stimulator controller. The controller box was installed inside the co-moving rack of the telescope. Red (double/single) lines show (AC/DC) power cables, black dashed lines show digital signal lines (Ethernet cable and USB cable are included), and green chain lines show (K-type) thermocouple leads.

horn) was placed on the heater and both sides of the gap. The diameter of the chopper wheel and horn aperture (diameter, 16 mm) were optimized to use the space in the box efficiently. The horn facing the heater was optimized to be a 10-mm aperture that maximally uses the area of the source heater. The horns were milled from aluminum blocks using an NC machine.

4.3 Modulation System

We adopted a rotation wheel chopper with a diameter of 160 mm, which was made of a 1-mm-thick aluminum plate. A stepping motor (Oriental motor PKP225) was employed to drive a chopper wheel. The chopping frequency (motor frequency times the number of blades, six) covered more than the sampling Nyquist frequency (152-Hz sampling). The IR optical encoder (OMRON EE-SX1140; 4 μ s both rising and falling times) was attached to read the chopper position. The encoder detected the timing when the chopper was in an open or closed position. The chopping information was combined with the clock at the microprocessor and sent to a housekeeping DAQ system, called “slowdaq.”

4.4 Control System

A diagram of the control system is shown in Fig. 4. A single-board computer (Raspberry Pi) was used as the main controller of the system. The control system was used for the following five functions: (1) to control the AC voltage supply (Kikusui PCR500M) to the heater. The voltage, current, and power from the AC supply were constantly monitored at 10-s intervals. (2) To transmit control signals to the stepping motor controller (Oriental Motor EMP401) for the chopper. (3) To communicate with the ADC module (LabJack U6 PRO), monitoring the temperature of the heater and inside the stimulator box using K-type thermocouples. (4) To receive chopper information from the microprocessor (Arduino Uno R3). The processor board calculates the chopper timing according to the IRIG-B timecode signal²⁷ and 16 MHz Arduino internal clock. (5) To distribute stimulator slowdaq information to the site Ethernet LAN.

4.5 Mechanical Design

The stimulator was assembled into a cubic casing of ~ 20 cm. Figure 5 shows the images under assembly. The casing had separate front and rear spaces. The front room contained only the stepping motor and cooling fans, and the rear room included the heater and others for temperature stability. The heater, inner cover, and support parts comprised the “heater unit,” which was accessible from the back of the stimulator. This design was adopted to easily replace the heater with a spare in case of failure of one heater. The stimulator was attached to a telescope, as shown in Fig. 6.

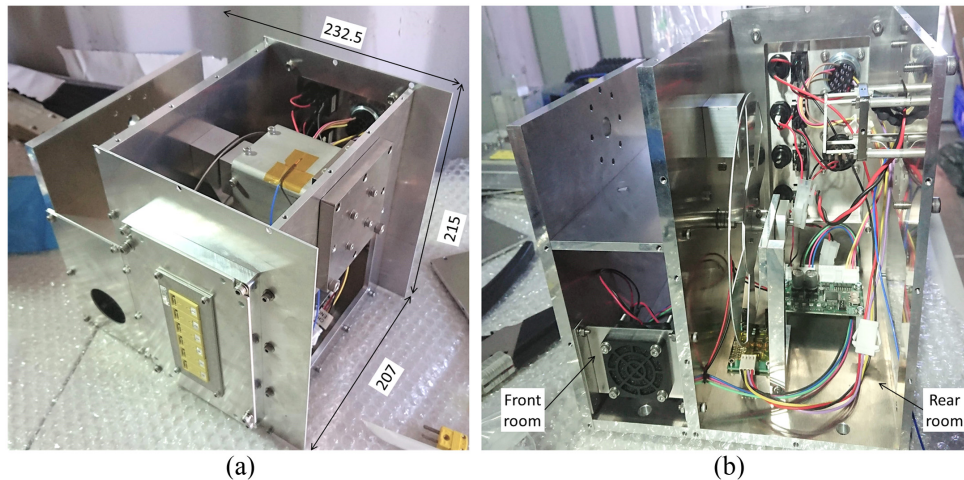


Fig. 5 Pictures of the stimulator in lab assembly. (a) Top panel and service window are disassembled. (b) A connector panel is removed; in addition, outer and inner heater covers are removed to show the heater structure.

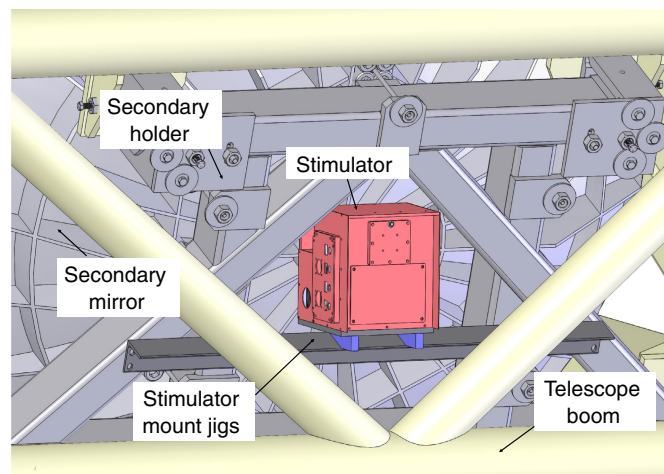


Fig. 6 Image depicting mounting of the stimulator on the telescope. The stimulator (painted in pink) is mounted on the base plate (dark gray). The base plate is attached to the insulating blocks (blue) and L-shaped angle beam. The L-shaped beam is bolted on the telescope's boom as well as the secondary mirror.

5 Operation Method

5.1 Hardware Operation

The sequence of stimulator calibration was controlled by the SA main control system.²⁸ The AC voltage supply for the heater was maintained at the nominal value. A discussion of the temperature stability is presented in Sec. 6.2.

Regular calibration runs with the stimulator were performed at the beginning and end of every 5 h of observation scans. In each run, the chopper was driven at seven different frequencies from low to high (5, 9, 13, 19, 29, 37, and 44 Hz), which were chosen referring to PB-1, not to collide with any other known modulation and noise frequencies (and their harmonics). The measurement time for each signal modulation frequency was set at 120 s. In some calibration runs, such as planet observations, the stimulator was used with a constant chopper frequency during the planet scan.

5.2 Data Analysis Method

The stimulator data were processed offline for each calibration runs. The time-ordered data were filtered using a high-pass filter and baseline subtraction at the beginning of the data analysis.

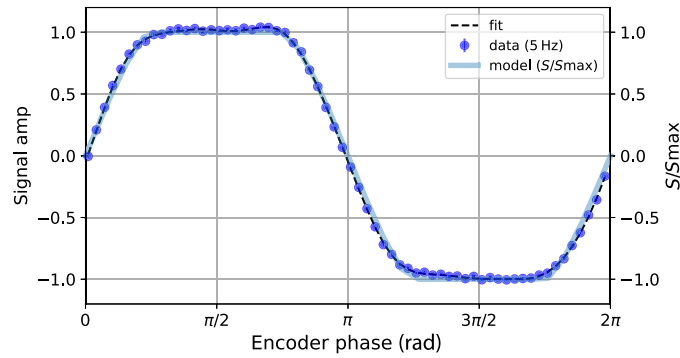


Fig. 7 Example of the measured stimulator signal waveform at 5 Hz. The time-ordered data are chunked and stacked using the encoder timing information. The signal waveform is fitted with a series of sinusoidal functions. The cross-sectional area of the light pipe beam²⁹ is also plotted as a model. The light pipe cross section and signal waveforms are in good agreement.

Subsequently, the time-ordered data were chunked and stacked with the encoder timing information for each chopper frequency. The amplitude of the modulated signal from the stimulator was estimated by fitting the stacked data, as shown in Fig. 7. We used a series of sinusoidal functions: $A(\theta) = \sum_{n=1}^7 A_n \sin(n\theta + \phi_n)$ [$0 \leq \theta < 2\pi$], where θ represents the phase of the chopper, and ϕ_n is the phase offset. Finally, the fitted A_1 value was inferred as the chopping amplitude.

6 Results from Validation Tests

The results of this study were based on data acquired during the early PB-2a commissioning period since the first light in January 2019.¹⁶ After installing the stimulator in the telescope, we evaluated the basic performance of the stimulator. In this section, we report the measurement of the signal intensity and the temperature stability of the stimulator, time constant, and gain calibration precision. The evaluated values are listed in Table 2.

6.1 Stimulator Signal Intensity

The intensity or effective temperature of the stimulator (T_{stm}) was obtained by observing the planets with known sky temperatures. During the scans of the planets, the modulation signal from the stimulator was introduced simultaneously. It is obtained by comparing the outputs from the stimulator (I_{stm}) and the planet through

Table 2 Summary of the measured characteristics of the stimulator. The signal effective temperature and source temperature fluctuation for one observation satisfy the required value listed in Table 1. The required value for the source temperature fluctuation is below the observed fluctuation without correction; in practice, the source temperature is corrected by monitoring. The source temperature fluctuation for the entire season is greater than the required value under no monitoring temperature conditions. However, in observations, heater temperature will be monitored and calibrated to satisfy fluctuation requirement.

Item	Measured value	Required value
Signal effective temperature T_{stm}	$46 \pm 8 \text{ mK}_{\text{RJ}}$ (90 GHz) $82 \pm 16 \text{ mK}_{\text{RJ}}$ (150 GHz)	>5 mK
Signal fluctuation $\delta T_{\text{stm}}/T_{\text{stm}}$	<0.45% (1 obs) <0.18% (1 season)	<0.66% (1 obs) <0.03% (1 season)
Modulation frequency $\delta f/f$	$\pm 0.2\%$	1%
Encoder timing δt_{chop}	$\sim 10 \mu\text{s}$	<0.1 ms

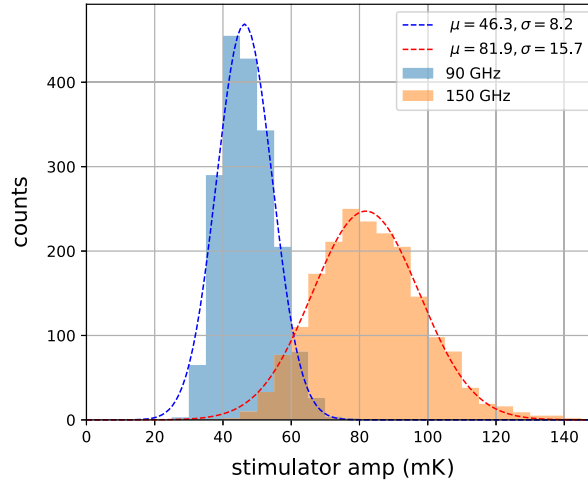


Fig. 8 Effective temperature of the stimulator for each bolometer.

$$T_{\text{stm}} = T_p \frac{\Omega_p I_{\text{stm}}}{I_p \Omega_{\text{beam}}}, \quad (9)$$

where T_p , I_p , and Ω_p are the brightness temperature, the measured amplitude, and solid angle of the planet, respectively. As a reference, we observed Jupiter, whose brightness temperature is $T_p = 174.1 \text{ K}_{\text{RJ}}$ at 143 GHz, and $T_p = 172.6 \text{ K}_{\text{RJ}}$ at 100 GHz.³⁰ The telescope beam size (Ω_{beam}) is calculated with 5.2 and 3.5 arc min (FWHM) for 90 and 150 GHz;¹⁶ hence the planets are regarded as a point source.

Across the focal plane, the calculated effective temperature of the stimulator was $46 \pm 8 \text{ mK}_{\text{RJ}}$ at 90 GHz and $82 \pm 16 \text{ mK}_{\text{RJ}}$ at 150 GHz, with 1σ spread, as shown in Fig. 8. Thus the measured effective temperature meets the requirements ($>5 \text{ mK}$) over the entire focal plane. (The signal is more significant than the PB-1 stimulator signal 18 to 43 mK_{RJ} ³¹ at the 150 GHz band.)

However, unknown systematic biases remain in the measured temperature. Large sources may come from the amplitude estimation and spectra of planet sources. For the amplitude estimation, 20% error remains in waveform fitting with conservative evaluation. For the spectra of planet sources, specifically the brightness temperature spectrum of Jupiter varied by 10 K at the maximum within the frequency ranges of 90 and 150 GHz bands,³⁰ and we assumed the same relative amount error in our sensor responsivity spectrum. In total $\sim 23\%$ of systematic error was estimated; however, the measured value still fulfilled the requirement, considering the worst assumption.

The stimulator is ideally an unpolarized light source, and its residual polarization should be sufficiently suppressed. After the stimulator was installed in the telescope, a HWP was placed between the stimulator and the receiver temporarily to assess the residual polarization of the stimulator's signal. Consequently, no obvious residual polarization signal of the stimulator above the current noise level was observed. The residual polarization was $\lesssim 3\%$ with the upper limit based on the noise level. This aspect should be evaluated in the future after improving the noise level.

6.2 Stimulator Signal Fluctuation

Subsequently, we evaluated the response of the bolometer output to changes in the heater temperature near the nominal temperature (750 to 960 K). The change in bolometer electrical output was $0.15 \pm 0.01\%/K$ to the change in the heater temperature. Because the shift in the heater temperature typically varies within 3 K during a single scan, the effect on the variation in responsivity of the bolometer output was $< 0.45\%$. This value satisfies the requirement of the temperature fluctuation ($< 0.66\%$).

Figure 9 shows the observed heater temperature. The RMS of the heater temperature for the total season was 1.7 K, and when the seasonal fluctuation was removed, the RMS was 1.0 K. The average day–night modulation was 1.4 K (max.–min.). These values are greater than the

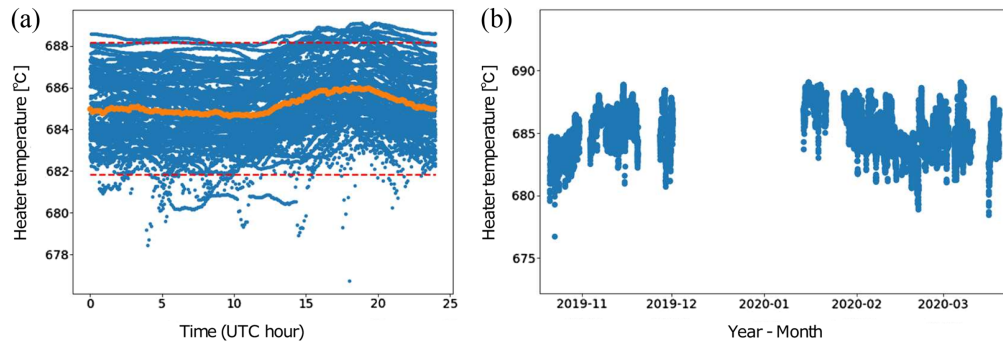


Fig. 9 (a) Observed heater temperature stacked in the 24-h range. The average is indicated using orange markers. The red dashed lines show the width of 0.66% power variation. (b) Temperature history after last heater modification.

required values for the entire season without correction. In the actual observations, the heater temperatures will be calibrated with the monitored values to satisfy the temperature fluctuation requirement. Requirement of 0.03% corresponds to 0.3 K for 960 K heater, and the precision of thermometry is better than this value.

The effect of reflection on the chopper (raised in Sec. 4.2) was verified using the data of the different heater voltages, particularly at 0 V. At this voltage, the detector observed a modulation signal between the heater at the ambient temperature and the chopper reflection, and approximately one-tenth of the signal was detected for the nominal voltage. The relative signal was not strongly dependent on the location of the detector, and the long-term fluctuation was confirmed in the discussion above. The magnitude of the 0-V signal can be understood as follows. The reflected light terminates at the environment apparatus, inside the receiver and the sky (the primary mirror).

6.3 Validation of Chopper and Encoder

The accuracy of the modulation frequency was typically 0.2%. The intrinsic stability of chopping was of the order of $10 \mu\text{s}$ (<0.1% relative value compared to highest chopping frequency). The overall spread was smaller than 1 ms in RMS when recorded at 5 Hz, the lowest chopper frequency (corresponding to 0.5% relative frequencies), which is dominated by the manufacturing imperfection of the chopper wheel. The intrinsic sensor jitter was estimated as $<1 \mu\text{s}$. The chopper frequency and readout timing requirements were confirmed to be satisfactory.

7 Demonstration of Calibration

7.1 Time Constant

The time constant of the bolometer was measured by changing the chopper frequencies and fitting for the value of the stimulator amplitude at each frequency. The one-pole model Eq. (6) used for fitting is shown as the response at frequency $A(f) = A_0[1 + (2\pi\tau f)^2]^{-1/2}$, where f is the modulation frequency, A_0 is the signal amplitude, and τ is the time constant of the bolometer. An example of the fitting of each bolometer response for each frequency is shown in Fig. 10.

In well-fabricated and properly tuned TESs, the resolution of the time constant $\delta\tau$ achieved ~ 0.01 ms for $\tau \sim 1$ ms (close to the design) case.³² The estimated A_0 was used for the relative gain calculation.

7.2 Gain Calibration Precision

Figure 11 presents a scatter plot of the precision of the gain and inverse of the signal-to-noise ratio. Noise is defined as the white noise value converted by the effective temperature of the stimulator's signal. The gain calibration precisions in the commissioning tests were 0.3% (90 GHz) and 0.2% (150 GHz) per observation. The gain calibration accuracy depends on the ratio of the gain to the statistical error obtained by fitting the response to the stimulator signal with the one-pole model, as in Sec. 7.1. The gain calibration precision improved as the noise level of the detector decreased, as indicated by Eq. (3). Based on the signal fluctuation evaluation test

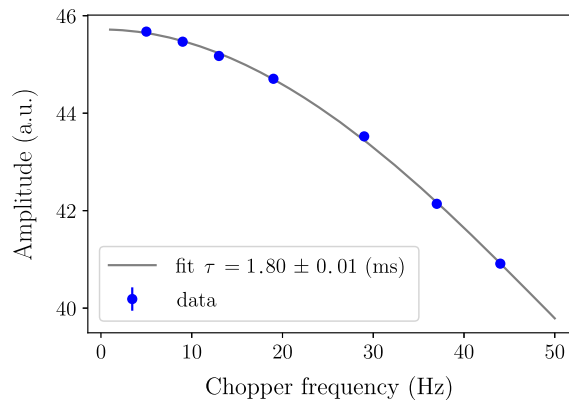


Fig. 10 Demonstration to measure the time constant on a typical TES at the observation site. The time constant is estimated by fitting with the one-pole model of Eq. (6).

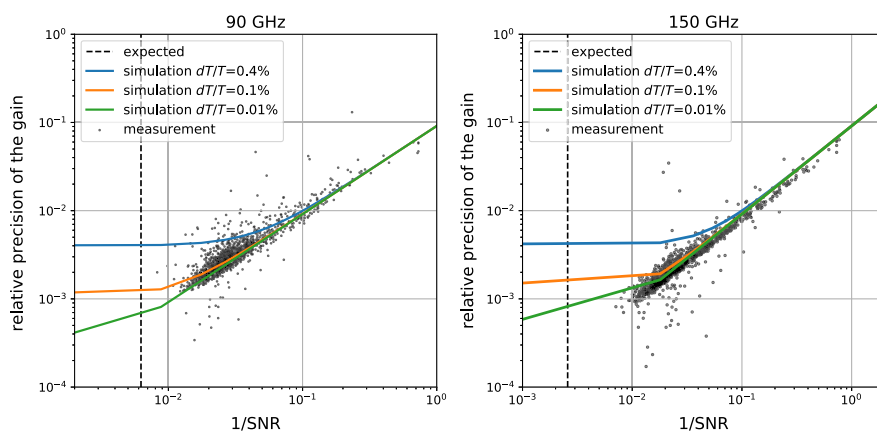


Fig. 11 Scatter plot of the ratio of the gain and the gain error (y axis) and inverse of signal-to-noise ratio (x axis) for each bolometer. The dashed vertical line shows the expected SNR. Curves indicate the relationships between SNR and gain precision, and the different colors denote the different assumed stimulator temperature variations. The trends of measured gain precision agree with model used for the estimation.

in Sec. 6.2, the signal fluctuation was $<0.45\%$. If the noise level is improved to the design value ($\text{NET}_{\text{bolo}} = 360 \mu\text{K}\sqrt{\text{s}}$), and signal fluctuation is 0.4% , the gain calibration accuracy of 0.4% (90 GHz) and 0.4% (150 GHz) are expected. At sufficiently low noise levels, the fluctuation of the heater source temperature limits the gain calibration precision. If $\delta T_{\text{stm}}/T_{\text{stm}} = 0.1\%$, the gain calibration precision is expected to be $\sim 0.1\%$ (90 GHz) and 0.2% (150 GHz).

8 Conclusion

Calibration of the detector gain is essential for CMB observations. We developed an advanced gain calibration system called a stimulator to perform periodic relative gain calibration of the TES for PB-2a. The system employed a thermal ceramic heater ($\sim 960 \text{ K}$) as a blackbody radiator to cover the entire frequency bands of the observation. In addition, a frequency-independent reflective horn allows simultaneous calibration at multiple frequencies. First, we established the requirements for the instrumental system based on the accuracy of the gain measurements in our experiment. This approach for estimating the requirements can be adapted for other CMB experiments. Early commissioning tests at an observation site in Chile confirmed that our system satisfied these requirements.

The stimulator contributes to the calibration of the detector gain for PB-2a observations. Furthermore, this calibration system applies to next-generation experiments with a larger number of bolometers and different observation frequencies, such as the Simons Observatory.^{33,34}

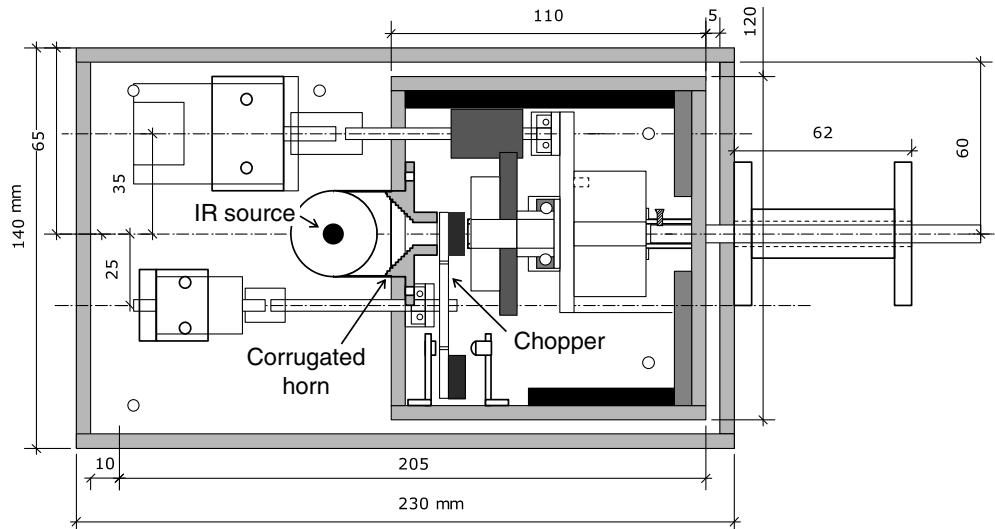


Fig. 12 Stimulator was used for PB-1. Radiation from IR source passes a corrugated horn, chopper, and a light pipe with a diameter of 1/4 in. A motor and an encoder system are equipped for the chopper.

9 Appendix A: PB-1 Stimulator

The stimulator that we referred to for the design in PB-2a was the one utilized in the PB-1 experiment. A schematic of the PB-1 stimulator is illustrated in Fig. 12. The basic components are similar to those of PB-2a.

For long-term observations, the heater source was replaced with a silicon nitride source (SUPCO Hot Surface Ignitor, SSN2000; maximum voltage, 120 V), which has a better environmental tolerance. The radiation from the heater was collected by a corrugated conical horn optimized for 150 GHz band. An optical chopper was located next to the horn. The chopper has two blades and comprises an aluminum plate with a foam-type blackbody (Eccosorb[®] AN series) applied on the receiver-side face. The chopper was driven by a low-torque stepping motor (Oriental Motor CMK235).

10 Appendix B: Derivation of Values of Requirements

10.1 Intensity-to-Polarization Leakage from Gain Mismatch

As mentioned in Sec. 3, gain miscalibrations result in systematic errors in CMB polarization measurements. The errors caused by the difference in gain calibration of two orthogonal detectors $\Delta\delta := \delta g_1 - \delta g_2$ in the power spectra of *E*-mode and *B*-mode polarizations are both $\langle (\Delta\delta)^2 \rangle f_1 \star C_\ell^{\text{TT}}$, where $f_1 (0 < f_1 < 1)$ is a parameter that depends on the scanning strategy of observation.³⁵ For example, when $\Delta\delta$ after averaging over detectors and observations is 1% and $f_1 = 1$, 10^{-4} of the power spectrum C_ℓ^{TT} originating from CMB temperature anisotropies leaks into both *E*-mode and *B*-mode polarizations. To mitigate the leakage from nonpolarized to polarized signal under 10% of the statistical uncertainty in the *B*-mode power spectrum, the difference in gain calibration $\Delta\delta/2$ must be calibrated to be $< 0.019\%$ ³⁶ after averaging over detectors and observations.

Assuming no systematic error from the instruments, the uncertainty of the gain for each pixel δg_{bolo} should be smaller than the fractional gain mismatch for a single observation. Here we are assuming 600-times constant elevation scan observations in a year, and the number of pixels N_{pixel} is 3600. From demand $\delta g_{\text{bolo}} < 39.5\%$ and Eq. (4), the signal intensity of stimulator T_{stm} must be larger than 0.1 mK. In addition, from $\delta g_{\text{array}} < 39.5\% / \sqrt{N_{\text{pixel}}}$ and Eq. (5), the signal fluctuation $\delta T_{\text{stm}} / T_{\text{stm}}$ must be $< 0.66\%$.

10.2 Monitoring Gain Variation During Observation

To accurately monitor the gain variation during scan observations, the signal fluctuation of the stimulator must be smaller than the gain-change uncertainty, denoted as δg_{scan} . Gain variation during observation can be caused by detector nonlinearity, where gain-change uncertainty can be expressed as $\delta g_{\text{scan}} = k\delta T_{\text{sky}}$. A temperature coefficient k is known to be $k = -1\%/K$, and the typical loading variation from sky δT_{sky} is ~ 1 K, from the PB-1 experiment data.³⁷ The uncertainty of the measured gain per observation δg_{bolo} must be $< \delta g_{\text{scan}} = 1\%$. According to Eq. (5), signal fluctuation $\delta T_{\text{stm}}/T_{\text{stm}}$ must be $< 1\%$. In addition, from Eq. (4), T_{stm} must be > 3 mK.

10.3 Designed Time Constant Value

We assume a simple case to estimate the time constant uncertainty. The estimated error is defined as $\delta\tau = (dI_{\text{obs}}/d\tau)^{-1}\delta I_{\text{obs}}$. From Eq. (6) and considering the maximum chopper frequency f_{max} , the estimated error of the time constant is

$$\delta\tau = \frac{(1 + (2\pi\tau f_{\text{max}})^2)^{3/2}}{(2\pi f_{\text{max}})^2 \tau G T_{\text{stm}}} \delta I_{\text{obs}} = \frac{(1 + (2\pi\tau f_{\text{max}})^2)^{3/2}}{(2\pi f_{\text{max}})^2 \tau} \frac{\text{NET}_{\text{bolo}}}{T_{\text{stm}} \sqrt{t_{\text{obs}}}}. \quad (10)$$

In accordance with Eq. (10), when the maximum signal modulation frequency f_{max} is 44 Hz, time constant value $\tau = 1$ ms, and required calibration accuracy $\delta\tau < 0.1$ ms, the required temperature intensity T_{stm} is higher than 5 mK.

10.4 Gain Error by Stimulator $<$ Absolute Gain Error

The calibration accuracy of the gain by the stimulator measurement must be better than the calibration accuracy of the absolute scale determined with CMB power spectrum C_{ℓ}^{TT} . The sample variance of the observable field in the universe limits the ultimate accuracy of the absolute scale:

$$\delta g_{\text{abs}} \approx (2\sqrt{N_{\text{mode}}})^{-1} \approx \left(2\sqrt{f_{\text{sky}} \sum_{\ell_{\text{min}}}^{\ell_{\text{max}}} (2\ell + 1)} \right)^{-1} \sim (2\sqrt{f_{\text{sky}} \ell_{\text{max}}})^{-1}, \quad (11)$$

where N_{mode} and f_{sky} denote the number of modes and the observable sky fraction (over 4π), respectively. The ℓ_{min} and ℓ_{max} in the summation indicate the minimum and maximum multipoles of the analysis window.

Based on the relationship described by Eq. (11) and assuming $f_{\text{sky}} = 65\%$ and $\ell_{\text{max}} = 2000$, δg_{abs} is $\sim 0.03\%$. From $\delta g_{\text{array}} < g_{\text{abs}} \sqrt{N_{\text{obs}}}$ and Eq. (5), signal fluctuation $\delta T_{\text{stm}}/T_{\text{stm}}$ must be $< 0.76\%$. From demand $\delta g_{\text{bolo}} < g_{\text{abs}} \sqrt{N_{\text{obs}} N_{\text{pixel}}}$ and Eq. (5), the required temperature intensity was $T_{\text{stm}} > 0.1$ mK.

10.5 Accuracy of the Time Constant Measurement for Chopper Frequency

Accuracy of the time constant depends on f_{max} , as seen in Eq. (10). We request the PB-2a stimulator to be able to cover that of the PB-1 stimulator: 44 Hz. The accuracy also depends on the uncertainty of chopper frequency. The error propagation on τ by the frequency error can be calculated using Eq. (6) as $\delta\tau/\tau = \delta f/f$. We require the chopper frequency uncertainty to be at the same level as the statistical uncertainty of the time-constant measurement (1% relative) in the entire chopper operation frequency.

10.6 Encoder Timing Readout

To properly use the stimulator modulation timing information, timing synchronization is required between the bolometer and stimulator DAQ systems. Therefore, the timing resolution is chosen to be substantially better than the chopping period at the maximum frequency, to avoid misidentifying one chopper's timing with another. The signal interval between opening and closing of the chopper is $t_{\text{chop}} = 1/2f_{\text{max}}$. Assuming $f_{\text{max}} = 44$ Hz and $t_{\text{chop}} \approx 10$ ms, the chopper timing resolution should be better than this number; for example, δt_{chop} shall be < 0.1 ms.

Table 3 System requirement summary for stimulator using HWP. We assumed the noise level $\text{NET}_{\text{bolo}} = 360 \mu\text{K}\sqrt{\text{s}}$ and measurement time $t_{\text{obs}} = 120 \text{ s}$. Here we assumed the temperature unit as the temperature after calibrating with the temperature of the blackbody spectrum of the CMB.

Item	Magnitude	Fluctuation	Section No.
(G) Optical leakage to $4f$ signal	$T_{\text{stm}} > 1 \text{ mK}$	$\delta T_{\text{stm}}/T_{\text{stm}} < 2.5\%$ (1 obs)	11.1
(H) Polarization angle error	$T_{\text{stm}} > 7 \text{ mK}$	—	11.2

11 Appendix C: Application of the Stimulator with Using HWP

SA uses a HWP in front of the receiver to mitigate $1/f$ noise.^{37,38} In the configuration with the HWP, as two linearly polarized components can be reconstructed from a single detector, other stimulator requirements are needed. Specifically, a new condition must be considered instead of item Sec. 10.1 in Appendix B. When linearly polarized light with a polarization angle of ϕ is incident to the rotating HWP at angle θ_{HWP} , the polarization angle of the transmitted light is $2\theta_{\text{HWP}} - \phi$. The polarization angle of the transmitted light rotates at $\theta_{\text{HWP}} = \omega_{\text{HWP}}t$ when the HWP rotates at a speed of ω_{HWP} . Therefore, the amplitude observed by the j 'th bolometer (whose sensitive polarization angle is ϕ_j) can be described as follows:

$$I_j = G_j \cdot [T + Q \cos(4\omega_{\text{HWP}}t - 2\phi_j) + U \sin(4\omega_{\text{HWP}}t - 2\phi_j)]. \quad (12)$$

For an ideal HWP, only the polarization components Q and U are modulated and not T .

11.1 Optical Leakage from Intensity to $4f$ Signal

This item is set to calibrate the optical leakage, that is, polarization converted from T component owing to imperfections of the optical elements on the sky side of the HWP, such as the primary mirror of the telescope. In PB-1, the optical leakage $\delta\lambda$ was estimated $\delta\lambda < 0.06\%$.³⁷ In PB-2a, we assume that $\delta\lambda$ is calibrated to be $< 0.01\%$. The uncertainty of optical leakage is estimated as $\delta\lambda \approx A^{(4)}\delta g/(\delta T_{\text{sky}}\sqrt{N_{\text{obs}}})$. Here we assume that the variation in sky temperature is $\delta T_{\text{sky}} \sim 1 \text{ K}$, the intensity of the 4th harmonic term of the HWP synchronous signal ($4f$ signal) is $A^{(4)} \sim 0.1 \text{ K}$ and the number of observation scan $N_{\text{obs}} = 600$ as used in Appendix B. Substituting values into the equation, the requirement for the detector gain δg is $< 2.5\%$. From Eq. (4), the signal intensity of stimulator T_{stm} must be larger than 1 mK . From Eq. (5), signal fluctuation $\delta T_{\text{stm}}/T_{\text{stm}}$ must be $< 2.5\%$.

11.2 Polarization Angle Error from the Time Constants Error

When there is uncertainty in the measurement time constant of the TES bolometer ($\delta\tau$), it leads to uncertainty in the polarization angle ($\delta\theta \approx 2\omega_{\text{HWP}}\delta\tau$). Uncertainty in the polarization angle induces an incorrect B -mode polarization pattern. To calibrate the polarization angle with accuracy $\delta\theta < 0.1 \text{ deg}$,³⁹ $\delta\tau$ must be calibrated to be $\delta\tau < \delta\theta/(2\omega_{\text{HWP}}) \approx 0.07 \text{ ms}$ with the HWP rotating at 2 Hz . Subsequently, the signal intensity of the stimulator T_{stm} should be $> 7 \text{ mK}$, as derived from Eq. (10).

Table 3 summarizes the requirements for the stimulator in applications using the HWP. As presented in Table 2, the stimulator also satisfies the required values for measurements using the HWP.

Code and Data Availability

The data utilized in this study were obtained by POLARBEAR Collaboration. Data are available from the authors upon request and with permission from POLARBEAR Collaboration.

Acknowledgments

This work was supported by Grant-in-Aid for JSPS Fellows (Grant No. JP19J10652), Ozaki Exchange Program 2019, and the SOKENDAI Advanced Research Course Program. This work was supported by World Premier International Research Center Initiative (WPI), MEXT, Japan and

JSPS Grants-in-Aid for Scientific Research (KAKENHI) (Grant Nos. 18H01240, 19KK0079, 19K14734, 22H04945, and 22K20371). The authors would like to thank T. Hamada and T. Fujino for the helpful comments and discussions. We also would like to thank S. Takayama (National Institute for Fusion Science) and T. Nojima (SAKAGUCHI ELECTRIC HEATERS CO., LTD.) for their technical advice on using the ceramic heater.

References

1. U. Seljak and M. Zaldarriaga, "Signature of gravity waves in the polarization of the microwave background," *Phys. Rev. Lett.* **78**, 2054–2057 (1997).
2. M. Kamionkowski, A. Kosowsky, and A. Stebbins, "A probe of primordial gravity waves and vorticity," *Phys. Rev. Lett.* **78**, 2058–2061 (1997).
3. D. J. Eisenstein, W. Hu, and M. Tegmark, "Cosmic complementarity: joint parameter estimation from cosmic microwave background experiments and redshift surveys," *Astrophys. J.* **518**, 2–23 (1999).
4. M. Kaplinghat, L. Knox, and Y.-S. Song, "Determining neutrino mass from the cosmic microwave background alone," *Phys. Rev. Lett.* **91**, 241301 (2003).
5. P. A. R. Ade et al., "A measurement of the cosmic microwave background b-mode polarization power spectrum at sub-degree scales with POLARBEAR," *Astrophys. J.* **794**, 171 (2014).
6. A. Hajian et al., "The Atacama cosmology telescope: calibration with the Wilkinson microwave anisotropy probe using cross-correlations," *Astrophys. J.* **740**, 86 (2011).
7. P. A. R. Ade et al., "Bicep2 III: instrumental systematics," *Astrophys. J.* **814**, 110 (2015).
8. R. J. Thornton et al., "The Atacama cosmology telescope: the polarization-sensitive actpol instrument," *Astrophys. J. Suppl. Ser.* **227**, 21 (2016).
9. Y. D. Takahashi et al., "Characterization of the bicep telescope for high-precision cosmic microwave background polarimetry," *Astrophys. J.* **711**, 1141–1156 (2010).
10. C. Bischoff et al., "The Q/U imaging experiment instrument," *Astrophys. J.* **768**, 9 (2013).
11. A. Suzuki et al., "The POLARBEAR-2 and the Simons Array experiments," *J. Low Temp. Phys.* **184**, 805–810 (2016).
12. N. Stebor et al., "The Simons Array CMB polarization experiment," *Proc. SPIE* **9914**, 99141H (2016).
13. M. Hasegawa et al., "POLARBEAR-2: a new CMB polarization receiver system for the Simons Array," *Proc. SPIE* **10708**, 1070802 (2018).
14. P. A. R. Ade et al., "Measurement of the cosmic microwave background polarization lensing power spectrum with the POLARBEAR experiment," *Phys. Rev. Lett.* **113**, 021301 (2014).
15. S. Adachi et al., "A measurement of the degree-scale CMB-mode angular power spectrum with POLARBEAR," *Astrophys. J.* **897**, 55 (2020).
16. D. Kaneko et al., "Deployment of POLARBEAR-2A," *J. Low Temp. Phys.* **199**, 1137–1147 (2020).
17. Y. Inoue et al., "POLARBEAR-2: an instrument for CMB polarization measurements," *Proc. SPIE* **9914**, 99141I (2016).
18. K. Irwin and G. Hilton, *Transition-Edge Sensors*, pp. 63–150, Springer Berlin Heidelberg, Berlin, Heidelberg (2005).
19. K. K. Schaffer et al., "The first public release of South Pole Telescope data: maps of a 95-square-deg field from 2008 observations," *Astrophys. J.* **743**, 90 (2011).
20. Z. Pan et al., "Optical characterization of the SPT-3g camera," *J. Low Temp. Phys.* **193**, 305–313 (2018).
21. Z. D. Kermish, "The POLARBEAR experiment: design and characterization," PhD thesis, University of California, Berkeley (2012).
22. J. Groh, "Design and deployment of the Simons Array cosmic microwave background polarization instrument," PhD thesis, University of California, Berkeley (2021).
23. P. A. R. Ade et al., "A measurement of the cosmic microwave background B-mode polarization power spectrum at subdegree scales from two years of POLARBEAR data," *Astrophys. J.* **848**, 121 (2017).
24. C. L. Bennett et al., "Nine-year Wilkinson microwave anisotropy probe (WMAP) observations: final maps and results," *Astrophys. J. Suppl. Ser.* **208**, 20 (2013).
25. P. A. R. Ade et al., "Joint analysis of BICEP2/Keck array and Planck data," *Phys. Rev. Lett.* **114**, 101301 (2015).
26. D. Barron et al., "Integrated electrical properties of the frequency multiplexed cryogenic readout system for POLARBEAR/Simons Array," *IEEE Trans. Appl. Supercond.* **31**(5), 1–5 (2021).
27. Timing Committee, Telecommunications and Timing Group, "Irig serial time code formats," IRIG STANDARD 200-16 (2016).
28. H. Nishino et al., "Data acquisition and management system for the CMB polarization experiment: Simons Array," *Proc. SPIE* **11453**, 1145329 (2020).
29. V. F. Duma, "Theoretical approach on optical choppers for top-hat light beam distributions," *J. Opt. A Pure Appl. Opt.* **10**, 064008 (2008).

30. Y. Akrami et al., “Planck intermediate results. LII. Planet flux densities,” *Astron. Astrophys.* **607**, A122 (2016).
31. D. Boettger, “CMB polarization measurements with the POLARBEAR experiment,” PhD thesis, University of California, San Diego (2017).
32. S. Takatori, “Calibration of detector time constant with a thermal source for the POLARBEAR-2A CMB polarization experiment,” APPC15 P1-as.02 (2022).
33. P. Ade et al., “The Simons Observatory: science goals and forecasts,” *J. Cosmol. Astropart. Phys.* **2019**, 56 (2019).
34. N. Galitzki et al., “The Simons Observatory: instrument overview,” *Proc. SPIE* **10708**, 1070804 (2018).
35. M. Shimon et al., “CMB polarization systematics due to beam asymmetry: impact on inflationary science,” *Phys. Rev. D* **77**, 083003 (2008).
36. F. T. Matsuda, “Cosmic microwave background polarization science and optical design of the POLARBEAR and Simons Array experiments,” PhD thesis, University of California, San Diego (2017).
37. S. Takakura et al., “Performance of a continuously rotating half-wave plate on the POLARBEAR telescope,” *J. Cosmol. Astropart. Phys.* **2017**, 008 (2017).
38. C. A. Hill et al., “Design and development of an ambient-temperature continuously-rotating achromatic half-wave plate for CMB polarization modulation on the POLARBEAR-2 experiment,” *Proc. SPIE* **9914**, 99142U (2016).
39. M. F. Navaroli et al., “Design and characterization of a ground-based absolute polarization calibrator for use with polarization sensitive CMB experiments,” *Proc. SPIE* **10708**, 107082A (2018).

Biographies of the authors are not available.